Hindawi Publishing Corporation
Journal of Nanomaterials
Volume 2014, Article ID 367529, 9 pages
http://dx.doi.org/10.1155/2014/367529

Research Article

Synthesis and Characterization of Europium-Doped Zinc Oxide Photocatalyst

Anukorn Phuruangrat,[1] Oranuch Yayapao,[2] Titipun Thongtem,[3] and Somchai Thongtem[2]

[1] *Department of Materials Science and Technology, Faculty of Science, Prince of Songkla University, Hat Yai, Songkhla 90112, Thailand*
[2] *Department of Physics and Materials Science, Faculty of Science, Chiang Mai University, Chiang Mai 50200, Thailand*
[3] *Department of Chemistry, Faculty of Science, Chiang Mai University, Chiang Mai 50200, Thailand*

Correspondence should be addressed to Anukorn Phuruangrat; phuruangrat@hotmail.com
and Somchai Thongtem; schthongtem@yahoo.com

Received 1 January 2014; Accepted 20 February 2014; Published 27 March 2014

Academic Editor: Abdelwahab Omri

Single crystalline flower-like ZnO and Eu-doped ZnO structures were successfully synthesized via a sonochemical method. Structures, morphologies, and photocatalytic activities of the as-synthesized samples were determined using X-ray diffraction, scanning electron microscopy, transmission electron microscopy, Raman spectroscopy, X-ray photoelectron spectroscopy, and ultraviolet-visible absorption spectroscopy. The photocatalytic activities of the as-synthesized samples were evaluated by the degradation of methylene blue in aqueous solutions under UV light. The photocatalytic results indicate that the as-synthesized Eu-doped ZnO shows good photocatalytic activity and could be considered as a promising photocatalyst for dye waste water treatment.

1. Introduction

In recent years, organic dyes in waste water have become one of the main pollutants in our daily lives. To solve this problem, semiconducting photocatalysts are the promising materials to degrade the organic pollutants in waste water because they proved to be the highly efficient catalysts for environmental remediation and energy conversion purposes [1, 2]. In photocatalytic process, valence band holes generated by photons from light source such as UV and visible light interact with H_2O or OH^- adsorbed on the catalytic surfaces to generate hydroxyl radical ($^{\bullet}OH$), and electrons in the conduction band interact with adsorbed O_2 to yield $^{\bullet}O_2^-$ radical. These radicals are highly reactive and unselective oxidants. Among them, ZnO and TiO_2 are the most extensively used photocatalysts due to their high photocatalytic activity and excellent chemical and mechanical stability and because they are nontoxic and inexpensive. Furthermore, ZnO is also a suitable alternative photocatalyst to TiO_2 because it is cheaper and has almost the same band gap energy. In addition, ZnO shows better performance compared to TiO_2 in the degradation of several organic contaminants in both acidic and basic media, which has stimulated many researchers to further explore the properties of ZnO in many photocatalytic reactions [3–5].

ZnO is a semiconductor with wide band gap of 3.37 eV and large exciton binding energy of 60 meV at room temperature, including excellent chemical and thermal stability. It has been widely used for optical, electrical, optoelectronic, catalytic, and photochemical properties, including optical waveguides and transparent conducting coatings [6–8]. It is the most important material to eliminate organic pollutants in waste water such as reactive brilliant red K-2BP [9], methylene blue [3, 4, 10], Acridine orange [5], rhodamine B [7, 10], methyl orange [11], and polyvinyl alcohol in aqueous solutions [12]. Sun et al. [3] reported that dumbbell-shaped ZnO photocatalyst showed a 99.6% decolorization efficiency of MB within 75 min under UV light (365 nm) which is higher than the commercial ZnO performance. Xu et al. [11] claimed that highly crystalline hexagonal ZnO nanorod assembled flowers, synthesized by a hydrothermal method, were able to significantly degrade methylene blue (MB) and rhodamine B (RhB) at 91% and 80% within 140 min. To improve photocatalytic activities, lanthanide ions with

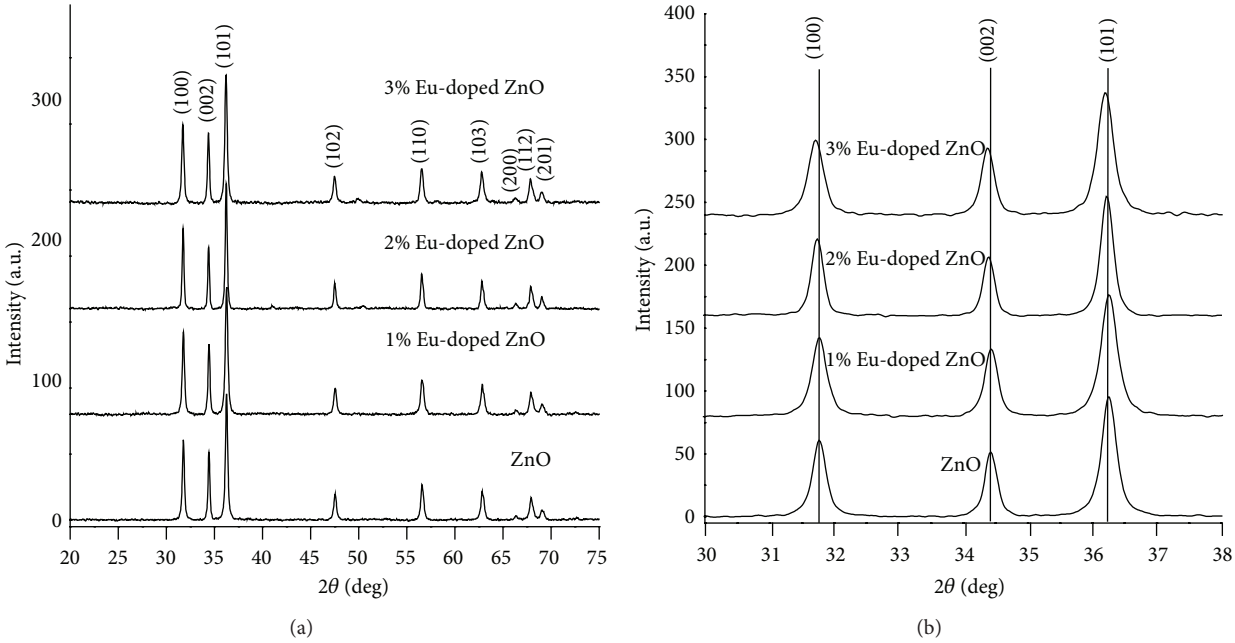

Figure 1: XRD patterns at 2θ of (a) 20°–75° and (b) 30°–38° of the as-synthesized undoped and Eu-doped ZnO samples synthesized by sonochemical method for 5 h.

4f electron configuration have been doped into ZnO to delay recombination rate of the electron-hole pairs and to effectively eliminate the organic dye pollutants in waste water [2]. The lanthanide ionic-doped ZnO, such as Sm^{3+}, Nd^{3+}, La^{3+}, Dy^{3+}, and Ce^{3+} [5, 8, 13–15], has been demonstrated to be more effective in promoting the photocatalytic activities than pure ZnO. Therefore, ZnO doped with Europium will be an efficient way to improve the photocatalytic activity, because the electrons are effectively trapped by the supplied chemical valence (Eu^{2+} and Eu^{3+}) sites [16].

In this work, the Eu-doped ZnO samples were synthesized by a sonochemical method. The photocatalytic activities of the as-synthesized samples for the methylene blue (MB) photodegradation were investigated and discussed.

2. Experimental Details

The zinc nitrate hexahydrate ($Zn(NO_3)_2{\cdot}6H_2O$), Europium nitrate hexahydrate ($Eu(NO_3)_3{\cdot}6H_2O$) as zinc and Europium sources, and sodium hydroxide (NaOH) were used without further purification.

To synthesize 0–3% Eu-doped ZnO, the 0.005 mole ($Zn(NO_3)_2{\cdot}6H_2O$) and 0–3 mol % $Eu(NO_3)_3{\cdot}6H_2O$ were dissolved in 100 mL deionized water under rigorous stirring until complete dissolution. Subsequently, 3 M NaOH solution was slowly dropped into these solutions until reaching at the pH 10 and the solutions became colorless. Then, the colorless solutions were sonicated in ultrasonic bath for 5 h. The precipitates were synthesized, filtered, washed with water and ethanol several times, dried, and collected for further characterization.

The products were characterized by X-ray diffraction (XRD) on a Philips X'Pert MPD X-ray diffractometer equipped with Cu K_α radiation over a range from 20° to 75° using a scanning rate of 0.02 deg/s. Morphologies of the samples were recorded by field emission scanning electron microscopy (FE-SEM) and transmission electron microscopy (TEM). FE-SEM images were carried out using a JEOL, JSM 6335F scanning electron microscope at 20 kV. TEM images were taken by a JEOL, JEM 2010 transmission electron microscope with an accelerating voltage of 200 kV. Raman spectra were recorded on a HORIBA JOBIN YVON T64000 spectrophotometer operated using 30 mW He-Ne red laser with 632.8 nm wavelength in the range of 100–1200 cm^{-1}. X-ray photoelectron spectroscopy (XPS) of the products was carried out via an Axis Ultra DLD, Kratos Analytical Ltd., with a monochromated Al K_α (1486.6 eV) radiation as the excitation source at 15 kV. All obtained spectra were calibrated to a C 1s electron peak at 285.1 eV.

Photocatalytic activities of the as-synthesized samples were tested by measuring the degradation of methylene blue (MB) in an aqueous solution under a UV radiation. Each 0.15 g photocatalyst was suspended in 100 mL of 10^{-5} M MB aqueous solutions, which were magnetically stirred for 60 min in the dark to establish an adsorption-desorption equilibrium of MB on the surface of the photocatalyst. Then the light was turned on to initiate the test. The solution was analyzed by a Lambda 25 spectrometer, using 450 W of Xe lamp with wavelength of 664 nm as maximum absorption of MB. Decolorization efficiency (%) was calculated using the following equation:

$$\text{Decolorization efficiency } (\%) = \frac{C_0 - C_t}{C_0} \times 100, \quad (1)$$

where C_0 is the initial concentration of MB and C_t is the concentration of MB after light irradiation.

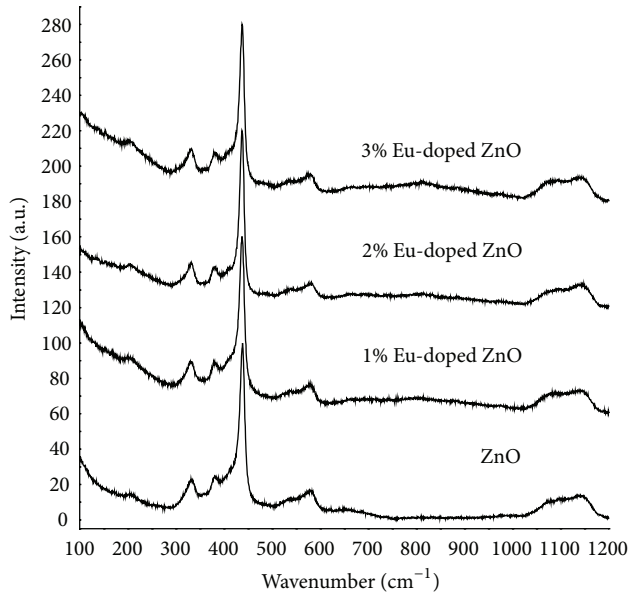

FIGURE 2: Raman spectra of the as-synthesized undoped and Eu-doped ZnO samples synthesized by sonochemical method for 5 h using He-Ne red laser with 632.8 nm wavelength.

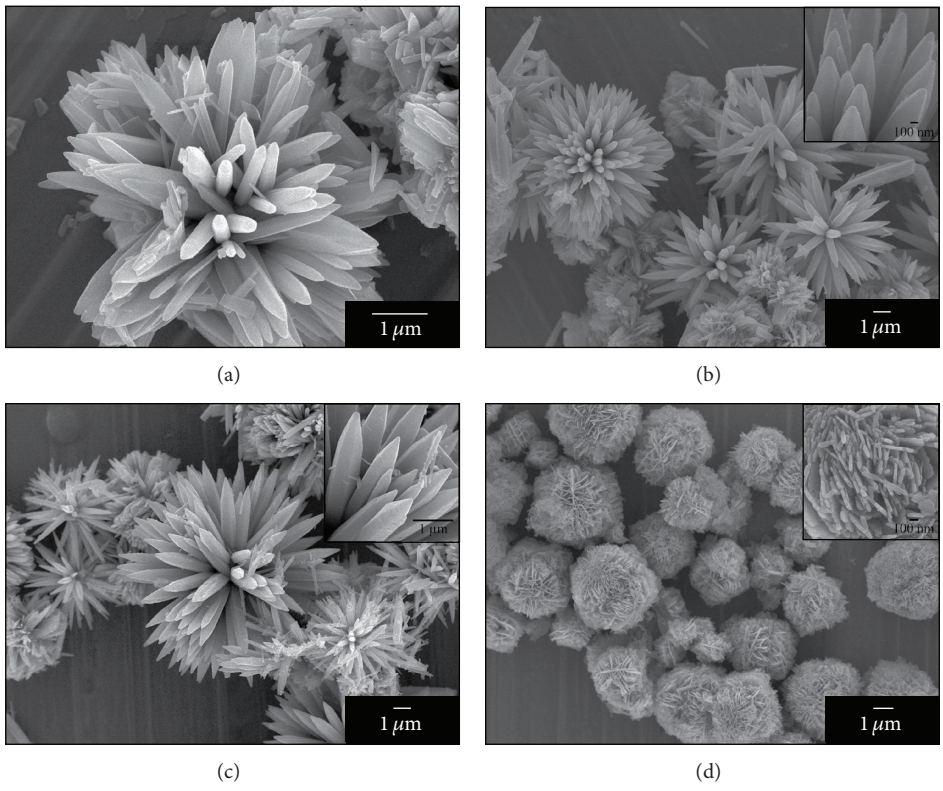

FIGURE 3: SEM images of (a) 0%, (b) 1%, (c) 2%, and (d) 3% of Eu-doped ZnO.

3. Results and Discussion

XRD patterns of $Zn_{1-x}Eu_xO$ (x = 0, 0.01, 0.02, and 0.03) synthesized by sonochemical radiation for 5 h are shown in Figure 1(a). The diffraction peaks of undoped ZnO sample appeared at 2θ = 31.80°, 34.46°, 36.28°, 47.58°, 56.62°, 62.88°, 66.40°, 68.00°, and 69.12° which were, respectively, identified to the (100), (002), (101), (102), (110), (103), (200), (112), and (201) diffraction planes of wurtzite hexagonal ZnO structure in accordance with the database of the JCPDS number 36–1451 [17]. However, the XRD patterns of $Zn_{1-x}Eu_xO$ (x = 0.01, 0.02, and 0.03) were still the same as that of pure

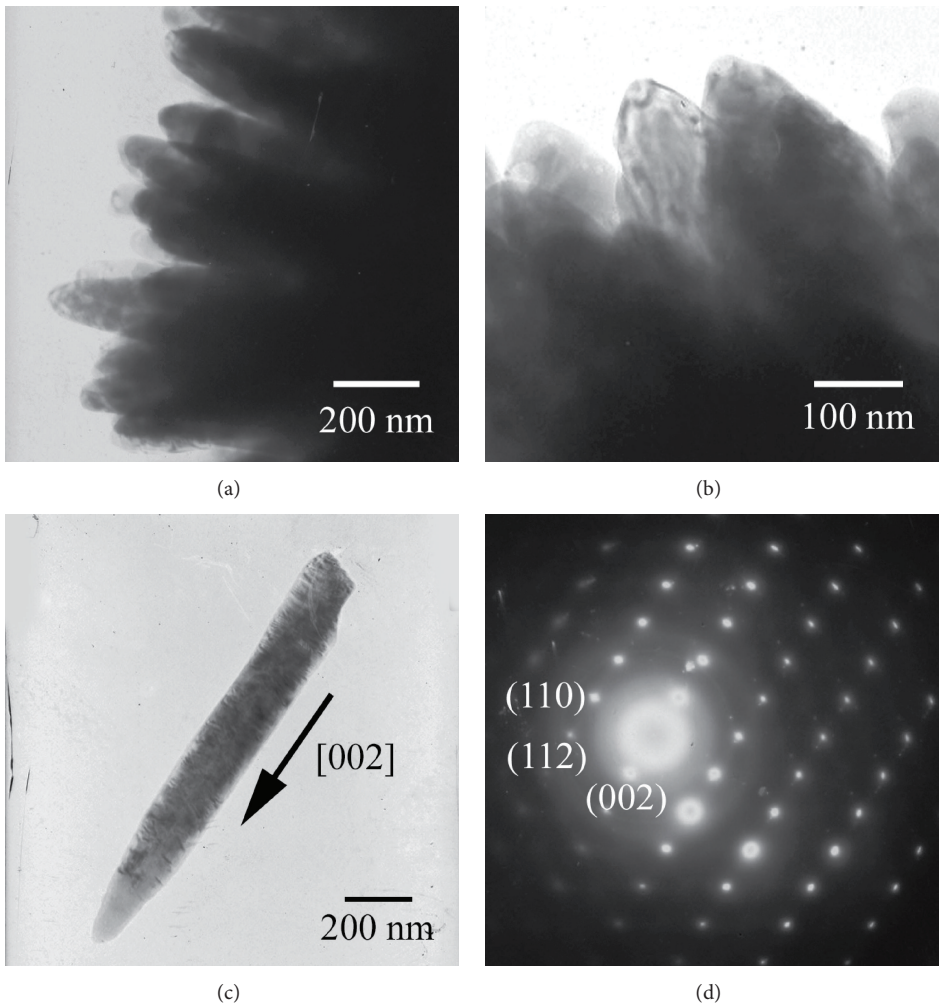

Figure 4: TEM images and SAED pattern of flowers of hexagonal pyramid tips ZnO nanorod.

wurtzite hexagonal ZnO structure without detection of any secondary phases. They indicated that Eu^{3+} ions of the doped ZnO samples were only incorporated in the ZnO lattice. The changes in the 2θ of the diffraction planes of (100), (002), and (101) peaks at $2\theta = 30.00^{\circ}$–38.00° for $Zn_{1-x}Eu_xO$ ($x = 0.01$, 0.02, and 0.03) with increasing concentration of Eu doping are shown in Figure 1(b). They shifted to lower 2θ due to the ionic radius of Eu^{3+} (0.95 Å) being larger than that of Zn^{2+} (0.74 Å) [18, 19].

Typical wurtzite ZnO belongs to the space group C_{6v}^4 with two formula units per primitive cell. A primitive ZnO cell has four atoms, each of which occupies C_{3v} sites, leading to 12 phonon branches (nine optical and three acoustic branches). Group theory predicts vibration modes at the zone center optical phonons: $A_1 + 2B_1 + E_1 + 2E_2$, where B_1 mode keeps silence and A_1, E_1 are polar modes, both Raman and IR active and thus split into transverse-optical (TO) and longitudinal-optical (LO) phonons, while two E_2 modes that denoted low-wavenumber E_{2L} and high-wavenumber E_{2H} modes are nonpolar. The E_{2L} mode is mainly associated with the vibration of the zinc sublattice, while the E_{2H} mode involves the oxygen motion and characteristic of the wurtzite structure. The B_1 mode is silent [20, 21].

Figure 2 shows the Raman spectra of the as-synthesized undoped and Eu-doped ZnO nanocrystals excited by red laser. Pure ZnO shows Raman peak at 439 cm^{-1} which is attributed to E_{2H} mode of the ZnO nonpolar optical phonons. The bands at 327 and 380 cm^{-1} are assigned as the $2E_{2L}$ and the TO mode with A_1 symmetry (A_{1T}), respectively [20]. The bands at 584 cm^{-1} correspond to E_1 symmetry with LO modes. Generally, the E_1(LO) peak is caused by defects due to O-vacancies, Zn-interstitials or these complexes, and free carriers [21, 22]. Moreover, the Raman peaks of E_{2H} evidently shift towards a low wavenumber from 439 cm^{-1} of undoped ZnO to 437 cm^{-1} of 3% Eu-doped ZnO [22], confirming an effective substitution of Zn^{2+} ions by Eu^{3+} ions in the as-synthesized nanocrystals, in accordance with the detection by the XRD analysis.

Morphologies of the pure and doped ZnO samples were characterized by FE-SEM as shown in Figure 3. In this research, the products are flower-like structures composed of hexagonal pyramid tips with edge length of 1.0–1.5 μm and

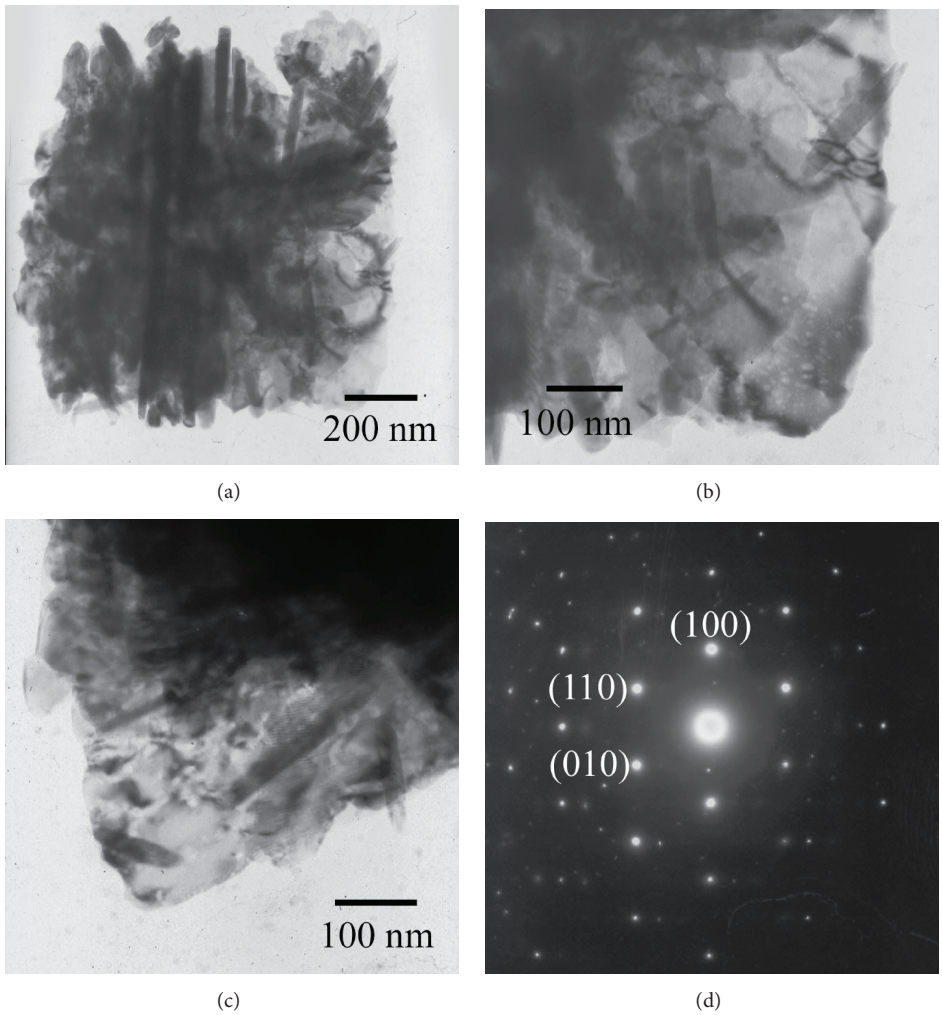

Figure 5: TEM images and SAED pattern of plate-like 3% Eu-doped ZnO flowers.

diameters of 200–500 nm, while a very small number of ZnO rods having diameters more than 500 nm were also observed. In the flower architecture, the rods fused together at one end and pointed out at the other end. Some dispersed rods were observed in the ZnO products as well. Each ZnO rod possessed the average diameter in the range of 250 ± 20 nm. Moreover, the hexagonal ZnO nanorods are tapered at their tips and exhibit clean and smooth surface throughout their lengths. However, SEM image of 3% Eu-doped ZnO presents two-dimension (2D) plate-like flower structure. It reveals that the detailed morphology of ZnO product is well-defined flower-like three-dimension (3D) structure with diameters in the range of 2–4 μm assembled by many densely arranged nanoplates as petals. A close-up view of the nanoplates-built flower-like nanostructures reveals that they are about 70 nm thick, and they alternately connect with each other to form a network-like surface of the flowers.

The flower-like rod-shaped profile was further characterized by a typical TEM image. The detailed morphological characterization of the as-synthesized hexagonal pyramid tip ZnO nanorods assembled flowers is further analyzed by TEM (Figure 4). They show the hexagonal pyramid tip ZnO nanorods which were assembled in flower clusters in consistent with the FE-SEM results in terms of their morphology and dimensions. A selected area electron diffraction (SAED) pattern of single hexagonal pyramid tip ZnO nanorod exhibiting a spot electron diffraction pattern. It confirms that single hexagonal pyramid tip ZnO nanorod is a single crystalline structure. SAED pattern was indexed to hexagonal wurtzite ZnO structure, preferentially grown along the [001] direction of hexagonal ZnO phase.

The morphological structure of 3% Eu-doped ZnO sample was further examined by TEM as shown in Figure 5. The TEM images further show that 3% Eu-doped ZnO sample is an irregular flower-like architecture, consistent with the SEM observation. TEM images taken from the edges of the individual structure (Figures 5(b) and 5(c)) reveal that the as-synthesized sample is highly crystallized and self-assembled with nanoplates. They are very thin and transparent to the electron beam. A SAED pattern shows an array of clear and regular diffraction spots of a single nanoplate, implying that the nanoplate is single-crystalline structure in nature. Thus,

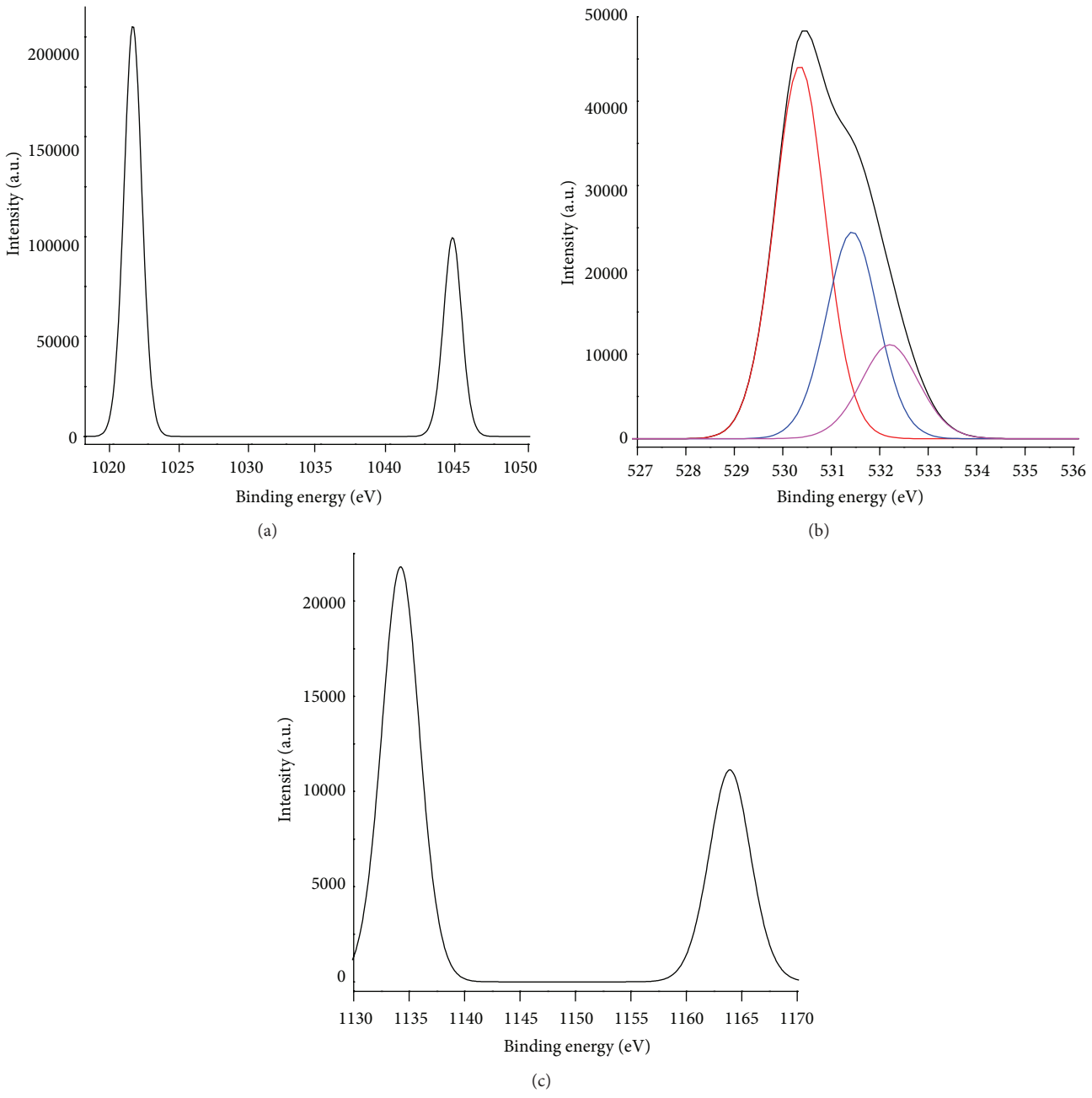

Figure 6: XPS spectra of (a) Zn 2p, (b) O 1s, and (c) Eu 3 d of 3% Eu-doped ZnO.

the formation of 3% Eu-doped ZnO hierarchical composites originates from the self-assembly of these single-crystalline nanoplates. The SAED was indexed to the (100), (110), and (010) planes of hexagonal ZnO structure which is normal to the horizontal plane of the hexagonal ZnO nanoplate. It is suggested that growth of the individual ZnO hexagonal nanoplates is along the six symmetric directions of ±[100], ±[110], and ±[010] but the typical growth along the [001] direction was suppressed [23–26], directly leading to the formation of hexagonal zinc oxide nanoplates.

XPS was used to characterize the detailed chemical composition of the 3% Eu-doped ZnO as shown in Figure 6 and was calibrated using the carbon peak (C-1s) at 285.1 eV as reference. Figure 6(a) shows the XPS spectra of the Zn-2p core level region. It shows doublet peaks at 1021.46 eV and 1044.53 eV, corresponding to the Zn $2p_{3/2}$ and $2p_{1/2}$ core levels, respectively [18, 27, 28]. Energy difference of the two peaks is 23.07 eV, which agrees well with the standard value of 22.97 eV, revealing the presence of Zn^{2+} ions in the oxide [18, 28]. The asymmetric feature observed in the O 1s peak at 530.6 eV is shown in Figure 6(b). It was deconvoluted by three subspectral components: stoichiometric ZnO (530.33 eV), chemisorbed oxygen on the sample (531.42 eV), and hydroxyl species on the sample (532.22 eV) [28, 29]. The Eu-3d XPS in

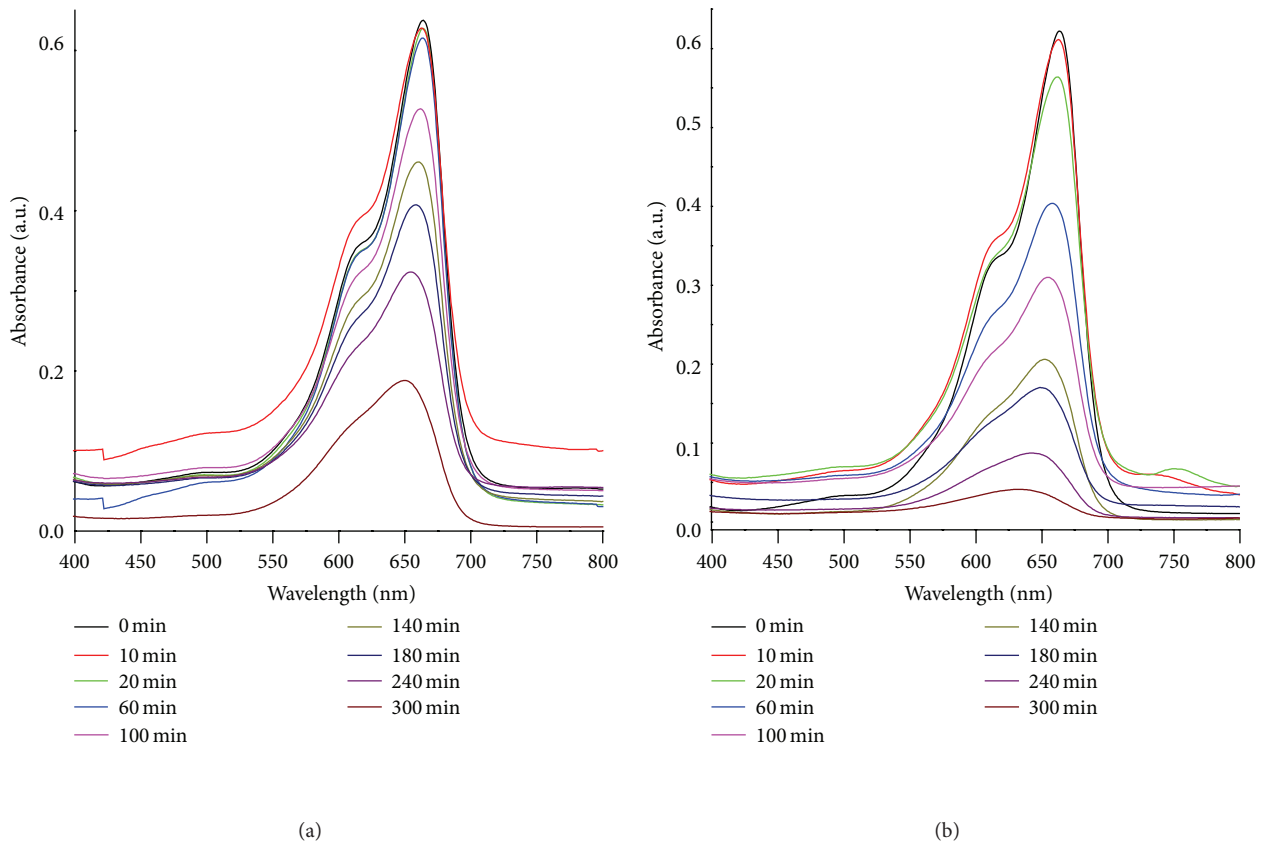

FIGURE 7: Vibration of the absorption spectra for MB solutions containing (a) undoped ZnO and (b) 3% Eu-doped ZnO under UV light for different time intervals.

the region of the Eu-doped ZnO nanorod samples is shown in Figure 6(c). These two doublet binding energy regions could be assigned to the Eu^{3+} $3d_{5/2}$ and $3d_{3/2}$ core levels at 1134.21 and 1163.90 eV [18, 27, 29]. The fact that only cationic Eu^{3+} species were detected in the sample suggests the incorporation of Eu^{3+} ions into the ZnO matrix.

The as-synthesized 0–3% Eu-doped ZnO samples are used as photocatalysts to study photocatalytic activity towards the efficient degradation of methylene blue (MB) as organic dye. Figure 7 shows the UV-visible absorption spectra of degraded MB over the undoped and 3% Eu-doped ZnO under UV light illumination within 0–300 min over the wavelength range of 400–800 nm. It can be seen that the maximum absorption at λ_{peak} = 664 nm of MB dye is continuously decreased with the increase of exposure time from 0 to 300 min. The decrease in the relative intensities of absorption of 3% Eu-doped ZnO is faster than that of pure ZnO which indicates that the Eu doping improves the effective performance degradation of dye under UV light illumination.

Figure 8(a) shows the photocatalytic activity of the undoped and Eu-doped ZnO samples. The blank experiment in the absence of photocatalyst demonstrated that MB was not photodegraded by the UV light. During photocatalysis, all the photocatalysts exhibited the photocatalytic activity in MB photodegradation under UV light irradiation, confirming that photocatalyst plays a role in the degradation of MB under UV light. ZnO is an effective photocatalyst in photodegradation of MB solution of 75.00%, lower in the photodegradation of the MB solution than Eu-doped ZnO. The 3% Eu-doped ZnO has the highest photocatalytic activity. The MB degradation efficiency of 3% Eu-doped ZnO reaches the 90.51%, which is 1.20 and 1.10 times higher than those of the pure ZnO and 1% Eu-doped ZnO, respectively.

Photocatalytic activity for degradation of MB obeys the pseudo-first-order reaction kinetics [1, 2, 10] with k as the rate constant and t as the UV irradiation time given by

$$C_t = C_0 e^{-kt}. \quad (2)$$

Figure 8(b) shows the plots of $\ln(C_0/C_t)$ versus the irradiation time for the photodegradation of MB. In this research, the photodegradation followed very well with the pseudo-first-order kinetics with R^2 = 0.9556, 0.9779, and 0.9959 for 0, 1, and 3% Eu-doped ZnO, respectively. The rate constants for degradation of MB on 0, 1, and 3% Eu-doped ZnO are 3.43×10^{-3}, 4.53×10^{-3}, and 7.73×10^{-3} min^{-1}, respectively. The rate constants for degradation of MB by 3% Eu-doped ZnO increase the reaction rate by about 2.25 times compared to pure ZnO. In general, performance activity of photocatalysts was determined by the delay of photogenerated electron-hole recombination rate. Therefore, enhancing the photocatalytic activity by doping ZnO nanostructure with a proper mole fraction of Eu^{+3} ions is attributed to increase in the electron-hole life time.

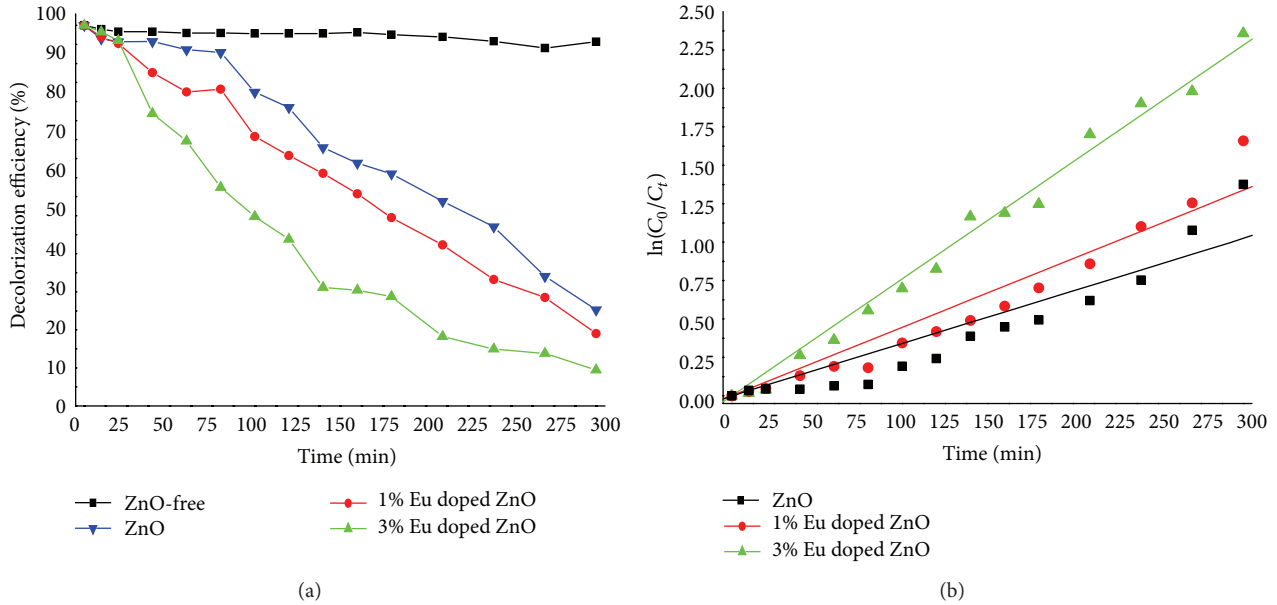

FIGURE 8: (a) Photodegradation efficiency and (b) reaction kinetics of the MB aqueous solutions of different percentages of Eu-doped ZnO under UV light within 300 min.

4. Conclusions

Single crystalline ZnO and Eu-doped ZnO have been successfully synthesized by a sonochemical process. The characterization results show that the as-synthesized ZnO and Eu-doped ZnO photocatalysts belong to the hexagonal wurtzite structure. The photocatalytic activities of the as-synthesized ZnO and Eu-doped ZnO photocatalysts have been evaluated by the degradation of MB in aqueous solutions under UV light. The MB decolorization efficiency of 3% Eu-doped ZnO is achieved at 90.51% within 300 min, higher than that of pure ZnO.

Conflict of Interests

The authors declare that there is no conflict of interests regarding the publication of this paper.

Acknowledgment

The authors are extremely grateful to the Prince of Songkla University, Thailand, under Contact no. SCI560495S.

References

[1] Y. Tian, L. Zhang, and J. Zhang, "A superior visible light-driven photocatalyst: europium-doped bismuth tungstate hierarchical microspheres," *Journal of Alloys and Compounds*, vol. 537, pp. 24–28, 2012.

[2] J. Xu, Y. Ao, D. Fu, and C. Yuan, "A simple route for the preparation of Eu, N-codoped TiO2 nanoparticles with enhanced visible light-induced photocatalytic activity," *Journal of Colloid and Interface Science*, vol. 328, no. 2, pp. 447–451, 2008.

[3] J.-H. Sun, S.-Y. Dong, Y.-K. Wang, and S.-P. Sun, "Preparation and photocatalytic property of a novel dumbbell-shaped ZnO microcrystal photocatalyst," *Journal of Hazardous Materials*, vol. 172, no. 2-3, pp. 1520–1526, 2009.

[4] M. Faisal, S. B. Khan, M. M. Rahman, A. Jamal, and M. M. Abdullah, "Fabrication of ZnO nanoparticles based sensitive methanol sensor and efficient photocatalyst," *Applied Surface Science*, vol. 258, pp. 7515–7522, 2012.

[5] S. B. Khan, M. Faisal, M. M. Rahman, and A. Jamal, "Low-temperature growth of ZnO nanoparticles: photocatalyst and acetone sensor," *Talanta*, vol. 85, no. 2, pp. 943–949, 2011.

[6] M. Khatamian, A. A. Khandar, B. Divband, M. Haghighi, and S. Ebrahimiasl, "Heterogeneous photocatalytic degradation of 4-nitrophenol in aqueous suspension by Ln (La^{3+}, Nd^{3+} or Sm^{3+}) doped ZnO nanoparticles," *Journal of Molecular Catalysis A*, vol. 365, pp. 120–127, 2012.

[7] J. Li, G. Lu, Y. Wang, Y. Guo, and Y. Guo, "A high activity photocatalyst of hierarchical 3D flowerlike ZnO microspheres: synthesis, characterization and catalytic activity," *Journal of Colloid and Interface Science*, vol. 377, pp. 191–196, 2012.

[8] J. C. Sin, S. M. Lam, K. T. Lee, and A. R. Mohamed, "Photocatalytic performance of novel samarium-doped spherical-like ZnO hierarchical nanostructures under visible light irradiation for 2, 4-dichlorophenol degradation," *Journal of Colloid and Interface Science*, vol. 401, pp. 40–49, 2013.

[9] Y. Liu, H. Lv, S. Li, X. Xing, and G. Xi, "Preparation and photocatalytic property of hexagonal cylinder-like bipods ZnO microcrystal photocatalyst," *Dyes and Pigments*, vol. 95, Article ID 443e449, 2012.

[10] Q. I. Rahman, M. Ahmad, S. K. Misra, and M. B. Lohani, "Hexagonal ZnO nanorods assembled flowers for photocatalytic dye degradation: growth, structural and optical properties," *Superlattices and Microstructures*, vol. 64, pp. 495–506, 2013.

[11] F. Xu, J. Chen, L. Guo, S. Lei, and Y. Ni, "In situ electrochemically etching-derived ZnO nanotube arrays for highly efficient and

facilely recyclable photocatalyst," *Applied Surface Science*, vol. 258, pp. 8160–8165, 2012.

[12] C. C. Lin and L. J. Hsu, "Removal of polyvinyl alcohol from aqueous solutions using P-25 TiO_2 and ZnO photocataysts: a comparative study," *Powder Technology*, vol. 246, pp. 351–355, 2013.

[13] O. Yayapao, S. Thongtem, A. Phuruangrat, and T. Thongtem, "Sonochemical synthesis, photocatalysis and photonic properties of 3% Ce-doped ZnO nanoneedles," *Ceramics International*, vol. 39, pp. S563–S568, 2013.

[14] O. Yayapao, T. Thongtem, A. Phuruangrat, and S. Thongtem, "Ultrasonic-assisted synthesis of Nd-doped ZnO for photocatalysis," *Materials Letters*, vol. 90, pp. 83–86, 2013.

[15] O. Yayapao, T. Thongtem, A. Phuruangrat, and S. Thongtem, "Sonochemical synthesis of Dy-doped ZnO nanostructures and their photocatalytic properties," *Journal of Alloys and Compounds*, vol. 576, pp. 72–79, 2013.

[16] S. Yao, C. Sui, and Z. Shi, "Preparation and characterization of visible-light-driven europium doped mesoporous titania photocatalyst," *Journal of Rare Earths*, vol. 29, no. 10, pp. 929–933, 2011.

[17] Powder Diffract, "File, JCPDS Internat," Centre Diffract, Data, PA, 19073-3273, USA, 2001.

[18] J. Yang, X. Li, J. Lang et al., "Synthesis and optical properties of Eu-doped ZnO nanosheets by hydrothermal method," *Materials Science in Semiconductor Processing*, vol. 14, no. 3-4, pp. 247–252, 2011.

[19] M. Wang, C. Huang, Z. Huang et al., "Synthesis and photoluminescence of Eu-doped ZnO microrods prepared by hydrothermal method," *Optical Materials*, vol. 31, no. 10, pp. 1502–1505, 2009.

[20] S. Husain, L. A. Alkhtaby, E. Giorgetti, A. Zoppi, and M. M. Miranda, "Effect of Mn doping on structural and optical properties of sol gel derived ZnO nanoparticles," *Journal of Luminescence*, vol. 145, pp. 132–137, 2014.

[21] P. S. Kumar, P. Paik, A. D. Raj et al., "Biodegradability study and pH influence on growth and orientation of ZnO nanorods via aqueous solution process," *Applied Surface Science*, vol. 258, pp. 6765–6771, 2012.

[22] N. K. Hassan and M. R. Hashim, "Flake-like ZnO nanostructures density for improved absorption using electrochemical deposition in UV detection," *Journal of Alloys and Compounds*, vol. 577, pp. 491–497, 2013.

[23] D. Chu, Y. Zeng, and D. Jiang, "Controlled growth and properties of Pb^{2+} doped ZnO nanodisks," *Materials Research Bulletin*, vol. 42, no. 5, pp. 814–819, 2007.

[24] C. X. Xu, G. P. Zhu, J. Kasim et al., "Spatial distribution of defect in ZnO nanodisks," *Current Applied Physics*, vol. 9, no. 3, pp. 573–576, 2009.

[25] M. Wang, S. H. Hahn, J. S. Kim, J. S. Chung, E. J. Kim, and K.-K. Koo, "Solvent-controlled crystallization of zinc oxide nano(micro)disks," *Journal of Crystal Growth*, vol. 310, no. 6, pp. 1213–1219, 2008.

[26] C. X. Xu, X. W. Sun, Z. L. Dong, and M. B. Yu, "Zinc oxide nanodlsk," *Applied Physics Letters*, vol. 85, no. 17, pp. 3878–3880, 2004.

[27] P. Mohanty, B. Kim, and J. Park, "Synthesis of single crystalline europium-doped ZnO nanowires," *Materials Science and Engineering B: Solid-State Materials for Advanced Technology*, vol. 138, no. 3, pp. 224–227, 2007.

[28] D. D. Wang, G. Z. Xing, J. H. Yang et al., "Dependence of energy transfer and photoluminescence on tailored defects in Eu-doped ZnO nanosheets-based microflowers," *Journal of Alloys and Compounds*, vol. 504, no. 1, pp. 22–26, 2010.

[29] J. Sin, S. Lam, I. Satoshi, K. Lee, and A. R. Mohamed, "Sunlight photocatalytic activity enhancement and mechanism ofnovel europium-doped ZnO hierarchical micro/nanospheres fordegradation of phenol," *Applied Catalysis B*, vol. 148-149, pp. 258–268, 2014.